Improved UFIR Filter for Fusing Recent INS-assisted Visual Measurement under Colored Measurement Noise in UAV Landing

YIDE ZHANG[1], TENG LI[1], XIN ZANG[1], JINGWEN YU[1], YUAN XU[1,*], YURIY S. SHMALIY[2]
[1]School of Electrical Engineering, University of Jinan, Jinan, CHINA
[2]Department of Electronics Engineering, Universidad de Guanajuato Salamanca, MEXICO
[*]Corresponding Author

Abstract: In this paper, we discuss the landing process of unmanned aerial vehicles (UAVs) employing inertial navigation system (INS) and visual measurement. Employing the integrated scheme, an improved unbiased finite impulse response (UFIR) filter is developed for fusing recent INS-assisted visual measurement under colored measurement noise (CMN). The UFIR filter developed for CMN and called cFIR filter is proposed, and then the hybrid UFIR/cFIR filter is developed to work in parallel. The Mahalanobis distance is used to select better results as the final result of the filter. It is shown experimentally that the proposed method enhances the accuracy and reliability of data fusion, thereby improving the overall performance of UAV autonomous landing systems.

Key-Words: Autonomous landing, Data fusion, UFIR filtering, Mahalanobis distance.

Received: March 13, 2023. Revised: March 15, 2024. Accepted: May 17, 2024. Published: June 6, 2024.

1 Introduction

Autonomous landing is a critical task for unmanned aerial vehicles (UAVs), [1], [2], [3], in various applications such as surveillance, [4], reconnaissance, [5], [6], and delivery, [7]. To achieve safe and precise landings, UAVs rely on a combination of sensors and algorithms to perceive their environment and make real-time decisions accurately, [8]. Many approaches have been proposed for localizing UAV. For example, [9], reports an absolute navigation of the landmark-based inertial measurement units (IMU)/Vision Navigation System (IMU/VNS) for UAV. One inertial navigation system (INS)-based integrated UAV localization has been proposed in [10]. In recent years, the use of April tags, also known as fiducial markers, has gained popularity in robotics and computer vision applications. These tags consist of unique visual patterns that can be easily detected and recognized by cameras, which can obtain the precise localization and tracking, [11]. Integrating April tag detection with IMU data during the autonomous landing process presents an opportunity to improve the accuracy and reliability of UAV navigation systems, [12].

Fusion of navigation information is a critical task in localization, [13], [14], [15]. One of the most accurate and robust solutions here is the unbiased finite impulse response (UFIR) filter, [16], which has found wide applications in a broad area of tracking, [17], [18]. In [19], the UFIR filter was extended to colored measurement noise (CMN) and analysed in detail in [16]. This opened new horizons for robust localization of moving objects in harsh environments, specifically for localization under harsh disturbances in the video camera bounding box, [16].

In this paper, we discuss the landing process of UAVs employing INS and visual measurement. Based on the integrated scheme, we improve the UFIR filter for fusion of recent INS-assisted visual measurement under CMN. The improved UFIR filters called cFIR filter is proposed. Then the UFIR and cFIR filters are united in a hybrid scheme, in which the *Mahalanobis* distance is used to select better results at the output. The experimental results demonstrate better performance of the proposed hybrid scheme.

2 INS-assisted visual UAV Landing system

In this section, we develop the INS-assisted visual landing system. The structure of the INS-assisted visual UAV landing system is shown in Fig. 1, where the visual sensor and the INS sensors are maintained on the UAV. The video camera is used to measure the position $\mathbf{Lo}_k^V$ and the attitude θ_k^V at the time index k. Meanwhile, the INS is used to measure the acceleration $\mathbf{a}_k$ and ω_k at the time index k. The $\mathbf{Lo}_k^V$, θ_k^V, $\mathbf{a}_k$, and ω_k are inputs of the UFIR/cUFIR filter, which is the main filter in this structure. We will consider it in detail later. The output of the FIR/cFIR filter is the UAV's position $\mathbf{Lo}_k$.

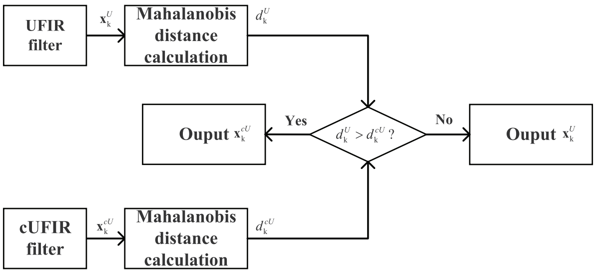

Figure 1: Structure of the INS-assisted visual UAV landing system.

The geometric relationships between the different sensors involved in the system are illustrated in Fig. 2, where (p_i^c, q_i^c) denotes the transformation from the camera coordinate system to the IMU coordinate system and represents the positional and orientational relationship between the camera and the IMU. In this system, the IMU is embedded within the camera, maintaining this relationship unchanged throughout motion and $\left(p_w^i, q_w^i\right)$ signifies the IMU's positional and orientational information in the world frame, expressing the IMU's position and orientation information in the global coordinate system (p_w^c, q_w^c).

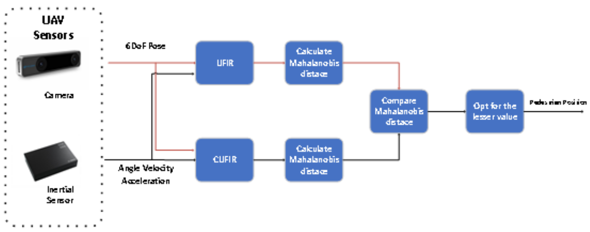

Figure 2: Visualization of the different coordinate frames in the setup.

3 Adaptive UFIR/cUFIR Filter

In this section, the adaptive UFIR/cUFIR filter will be derived. First, the data fusion model will be proposed. Then, the cUFIR filter will be developed based on the data fusion model. Finally, the adaptive UFIR/cUFIR filter will be presented.

3.1 Data Fusion Model for INS-assisted Visual UAV Landing

We use the 9-dimensional state vector

$$\mathbf{x}_k = \begin{bmatrix} \mathbf{Lo}_k & \mathbf{Vel}_k & \theta_k \end{bmatrix}^T , \tag{1}$$

which includes the 3-dimensional position, velocity and attitude, and where $\mathbf{Lo}_k$ represents the position at the time index k, $\mathbf{Vel}_k$ denotes the velocity of the UAV, and θ_k is the attitude, which includes 3 Euler angle. The state equation adopted in this work is as follows:

$$\mathbf{x}_k^- = \mathbf{S}_k \mathbf{x}_k + \varpi_k \, , \tag{2}$$

where the following matrices are used:

$$\mathbf{S}_k = \begin{bmatrix} \mathbf{I}_{3\times3} & \begin{bmatrix} \Delta t & 0 & 0 \\ 0 & \Delta t & 0 \\ 0 & 0 & \Delta t \end{bmatrix} & \mathbf{A} \\ \mathbf{0}_{3\times3} & \mathbf{I}_{3\times3} & \mathbf{B} \\ \mathbf{0}_{3\times3} & \mathbf{0}_{3\times3} & \mathbf{C} \end{bmatrix} , \tag{3}$$

$$\mathbf{A} = -\mathcal{T}_{(\mathbf{q}_k)}^T \lfloor \mathbf{a}_k \rfloor \left(\frac{\Delta t^2}{2} - \frac{\Delta t^3}{3!} \lfloor \omega_k \rfloor + \frac{\Delta t^4}{4!} \lfloor \omega_k \rfloor^2 \right) , \tag{4}$$

$$\mathbf{B} = -\mathcal{T}_{(\mathbf{q}_k)}^T \lfloor \mathbf{a}_k \rfloor \left(\Delta t - \frac{\Delta t^2}{2!} \lfloor \omega_k \rfloor - \frac{\Delta t^3}{3!} \lfloor \omega_k \rfloor^2 \right) , \tag{5}$$

$$\mathbf{C} = \mathbf{I}_{3\times3} - \Delta t \lfloor \omega_k \rfloor + \frac{\Delta t^2}{2!} \lfloor \omega_k \rfloor^2 , \tag{6}$$

where $\mathbf{S}_k$ denotes the state transition matrix, $\varpi_k \sim \mathcal{N}(0, \mathbf{Q}_k)$ is the system noise, the matrices $\lfloor \omega_k \rfloor$ and $\lfloor \mathbf{a_k} \rfloor$ are skew-symmetric matrices corresponding to ω_k and $\mathbf{a_k}$ respectively, $\mathcal{T}(\mathbf{q}_k)^T$ is used as the rotation matrix corresponding to the quaternion $\mathbf{q}_k$, which are shown as follows:

$$\lfloor \mathbf{a}_k \rfloor = \begin{bmatrix} 0 & -a_{z,k} & a_{y,k} \\ a_{z,k} & 0 & -a_{x,k} \\ -a_{y,k} & a_{x,k} & 0 \end{bmatrix} , \tag{7}$$

$$\lfloor \omega_k \rfloor = \begin{bmatrix} 0 & -\omega_{z,k} & \omega_{y,k} \\ \omega_{z,k} & 0 & -\omega_{x,k} \\ -\omega_{y,k} & \omega_{x,k} & 0 \end{bmatrix} , \tag{8}$$

where $(\omega_{x,k}, \omega_{y,k}, \omega_{z,k})$ is the acceleration in body-frame (b-frame), $(\omega_{x,k}, \omega_{y,k}, \omega_{z,k})$ is the angular velocity in b-frame. Thus, the observation equation of the data fusion model used in this work can be listed as follows:

$$\mathbf{y}_k = \mathbf{H}\mathbf{x}_k + \upsilon_k \, , \tag{9}$$

where $\mathbf{y}_k = \begin{bmatrix} \hat{\mathbf{L}}\mathbf{o}_k & \hat{\theta}_k \end{bmatrix}^T$ represents the observation vector, and $\hat{\mathbf{L}}\mathbf{o}_k$ and $\hat{\mathbf{L}}\mathbf{o}_k$ are measured by the camera directly. And $\mathbf{H} = \begin{bmatrix} \mathbf{I}_{3\times3} & \mathbf{0}_{3\times3} & \mathbf{0}_{3\times3} \\ \mathbf{0}_{3\times3} & \mathbf{0}_{3\times3} & \mathbf{I}_{3\times3} \end{bmatrix}$ serves as the observation matrix, $\upsilon_k \sim \mathcal{N}(0, \mathbf{R}_k)$ is the measurement noise.

Noted that the variable υ_k represents the measurement noise at time k. In the current mainstream methods, it is common to assume the measurement noise as Gaussian white noise. However, ensuring the persistent nature of white noise in practical applications poses challenges, [20]. To address this issue, the Gauss-Markov model is proposed for υ_k as follows:

$$\xi_k = \Theta_k \xi_{k-1} + \upsilon_k \,, \tag{10}$$

where ξ_k is the colored CMN, Θ_k is the coloredness coefficient, and υ_k is white Gaussian driving noise with known covariance. To transform the model $\mathbf{y}_k$ with CMN wo another one with white Gaussian noise, we use Bryson's measurement differencing, [21], [22], and write the new observation $\mathbf{m}_k$ as

$$\mathbf{m}_k = \mathbf{y}_k - \Theta_k \mathbf{y}_{k-1} = \mathbf{O}_k \mathbf{x}_k + \bar{\upsilon}_k \,, \tag{11}$$

where $\mathbf{O}_k = \mathbf{H}_k - \Pi_k$, $\Pi_k = \Theta_k \mathbf{H}_{k-1} \mathbf{S}_k^{-1}$, $\bar{\upsilon}_k = \Pi_k \varpi_k + \upsilon_k$. The UFIR/cUFIR filtering algorithm will be developed next.

3.2 Adaptive UFIR/cUFIR filter

Using the above-discussed state space model, the UFIR/cUFIR filtering algorithm can be developed as in the following. First, we list the standard UFIR filtering algorithm represented with the pseudo code as Algorithm 1.

Algorithm 1: Standard UFIR Filtering Algorithm

Data: $\mathbf{y}_k$, $\hat{\mathbf{x}}_0^U$
Result: $\hat{\mathbf{x}}_k^U$
begin
  for $k = L-1 : \infty$ **do**
    $l_1 = k - L + D_U$
    $\mathbf{G}_{l_1}^U = \mathbf{I}$;
    $\tilde{\mathbf{x}}_{l_1} = \begin{cases} \mathbf{y}_{l_1}, l_1 < L_U - 1 \\ \hat{\mathbf{x}}_{l_1}^U, l_1 \geq L_U - 1 \end{cases}$;
    for $j = l_1 + 1 : k$ **do**
      $\tilde{\mathbf{x}}_j^{U-} = \mathbf{S}_j \tilde{\mathbf{x}}_j^U$;
      $\mathbf{G}_j^U = \left[\mathbf{H}^T\mathbf{H} + (\mathbf{S}\mathbf{G}_{j-1}^U\mathbf{S}^T)^{-1}\right]^{-1}$;
      $\mathcal{F}_j^U = \mathbf{G}_j^U \mathbf{H}^T$;
      $\tilde{\mathbf{x}}_j^U = \tilde{\mathbf{x}}_j^- + \mathcal{F}_j^U[\mathbf{y}_k - \mathbf{H}\tilde{\mathbf{x}}_j^{U-}]$;
    end for
    $\hat{\mathbf{x}}_k^U = \tilde{\mathbf{x}}_j^U$;
  end for
end
† D_U is the size of the filter

Now we recall that the Kalman filter relies on white Gaussian noise in the system and in the measurement. In practical applications, CMN can affect its accuracy significantly, and therefore the UFIR approach is more preferable. A pseudo code of the proposed cUFIR filter operating in the presence of CMN is listed as Algorithm 2.

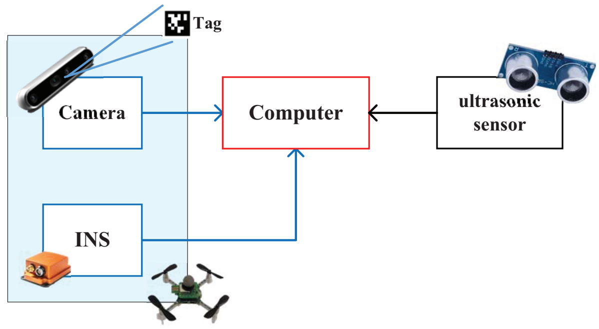

Figure 3: Structure of the adaptive UFIR/cUFIR filter.

Algorithm 2: cUFIR Filtering Algorithm

Data: $\mathbf{y}_k$, $\hat{\mathbf{x}}_0^{cU}$
Result: $\hat{\mathbf{x}}_k^{cU}$
begin
  for $k = L-1 : \infty$ **do**
    $l_1 = k - L + D_U$
    $\mathbf{G}_{l_1}^{cU} = \mathbf{I}$;
    $\tilde{\mathbf{x}}_{l_1}^{cU} = \begin{cases} \mathbf{y}_{l_1}, l_1 < L_U - 1 \\ \hat{\mathbf{x}}_{l_1}^{cU}, l_1 \geq L_U - 1 \end{cases}$;
    for $j = l_1 + 1 : k$ **do**
      $\mathbf{m}_k = \mathbf{y}_k - \Theta_k \mathbf{y}_{k-1}$;
      $\tilde{\mathbf{x}}_j^{cU-} = \mathbf{S}_j \tilde{\mathbf{x}}_j^{cU}$;
      $\mathbf{G}_j^{cU} = \left[\mathbf{O}^T\mathbf{O} + (\mathbf{S}\mathbf{G}_{j-1}^{cU}\mathbf{S}^T)^{-1}\right]^{-1}$;
      $\mathcal{F}_j^{cU} = \mathbf{G}_j \mathbf{O}^T$;
      $\tilde{\mathbf{x}}_j^{cU} = \tilde{\mathbf{x}}_j^{cU-} + \mathcal{F}_j^{cU}[\mathbf{m}_k - \mathbf{O}\tilde{\mathbf{x}}_j^{cU-}]$;
    end for
    $\hat{\mathbf{x}}_k^{cU} = \tilde{\mathbf{x}}_j^{cU}$;
  end for
end

The adaptive UFIR/cUFIR filter is developed for the structure shown in Fig. 3 as follows. We employ the *Mahalanobis* distance to verify the performances of the UFIR filter and the cUFIR filter by using the following equations:

$$d_k^U = (\mathbf{y}_k - \mathbf{H}\bar{\mathbf{x}}_{\mathbf{k}}^{U-})^T \mathbf{R}_k (\mathbf{y}_k - \mathbf{H}\bar{\mathbf{x}}_{\mathbf{k}}^{U-}) \,, \tag{12}$$

$$d_k^{cU} = (\mathbf{m}_k - \mathbf{O}\bar{\mathbf{x}}_{\mathbf{k}}^{cU-})^T \mathbf{R}_k (\mathbf{m}_k - \mathbf{O}\bar{\mathbf{x}}_{\mathbf{k}}^{cU-}) \,, \tag{13}$$

where d_k^U and d_k^{cU} are the *Mahalanobis* distances. Then we use the following conditions: if $d_k^U > d_k^{cU}$,

Figure 4: Structure of the measurement test equipment.

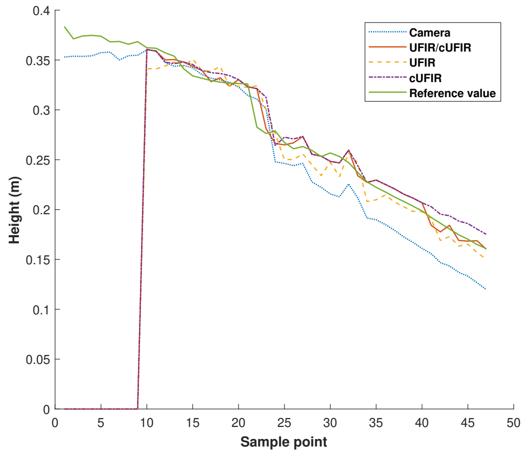

Figure 5: The UAV used in this work.

then $\hat{\mathbf{x}}_k^U$ goes to the output; otherwise, $\hat{\mathbf{x}}_k^{cU}$ goes to the output. A pseudo code of the adaptive hybrid UFIR/cUFIR filter is listed as Algorithm 3.

Algorithm 3: Adaptive Hybrid UFIR/cUFIR Filtering Algorithm

Data: $\mathbf{y}_k$, $\hat{\mathbf{x}}_0^U$, $\hat{\mathbf{x}}_0^{cU}$
Result: $\hat{\mathbf{x}}_k$
begin
  for $k = L-1 : \infty$ **do**
    Get $\hat{\mathbf{x}}_k^U$ by using Algorithm 1;
    $d_k^U = (\mathbf{y}_k - \mathbf{H}\bar{\mathbf{x}}_{\mathbf{k}}^{U-})^T \mathbf{R}_k (\mathbf{y}_k - \mathbf{H}\bar{\mathbf{x}}_{\mathbf{k}}^{U-})$;
    Get $\hat{\mathbf{x}}_k^{cU}$ by using Algorithm 1;
    $d_k^{cU} = (\mathbf{m}_k - \mathbf{O}\bar{\mathbf{x}}_{\mathbf{k}}^{cU-})^T \mathbf{R}_k (\mathbf{m}_k - \mathbf{O}\bar{\mathbf{x}}_{\mathbf{k}}^{cU-})$;
    if $d_k^U < d_k^{cU}$ **then**
      $\hat{\mathbf{x}}_k = \hat{\mathbf{x}}_k^U$;
    else
      $\hat{\mathbf{x}}_k = \hat{\mathbf{x}}_k^{cU}$;
    end if
  end for
end

4 Experimental Results

In this section, we test the filters developed by real experimental data. First, we tune the filters and then analyse filtering results.

4.1 Hardware Setting

The structure of the experimental test used in this work is shown in Fig. 4. In the testing, a visual camera is used to measure the UAV's attitude and the distance between the UAV and the tag. Meanwhile, the INS is used to measure the $\mathbf{a}_k$ and ω_k. The hight of the UAV is consider in this work, thus we employ an ultrasonic sensor to measure the distance between the UAV and the floor, which is denoted as the reference value.

In our experiments, we utilize the Z410 UAV as the data acquisition platform. The UAV is equipped with the Pixhawk 2.4.8 flight controller and the M8N GPS module. Additionally, a Raspberry Pi 3B+ onboard computer is used, which enables the external control of the UAV through programming languages such as Dronekit-Python, ROS, and OpenCV. An Intel T265 stereo camera is incorporated into the system. Developed by Intel, the T265 camera features two fisheye lenses, each with an approximate field of view of 170 degrees. The T265 camera is equipped with an integrated Inertial Measurement Unit (IMU) utilizing Bosch's BMI055 sensor. The UAV used in this work is shown in Fig. 5.

4.2 Performance Evaluation

Fig. 6 displays the height measured by the camera, UFIR filter, cUFIR filter, and UFIR/cUFIR filter, Along, we show the reference value in the test. In this figure, the reference value is denoted by the green line, the camera solution is denoted by the blue line, the orange line means the UFIR filtering solution, the cUFIR filtering solution is denoted by the purple line, and the proposed UFIR/cUFIR filter is denoted by the red line. From this figure, we see that the heights provided by the UFIR filter, cUFIR filter, and the UFIR/cUFIR filter have dead zones, and that their outputs range close to the reference value. Both the UFIR and the cUFIR filtering solutions range closer to the reference value. The height estimated by the pro-

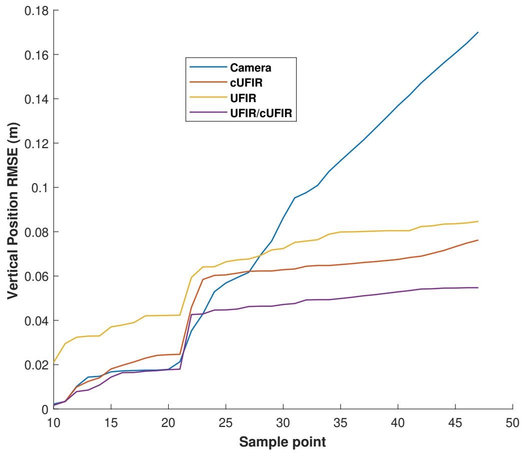

Figure 6: The heights measured by the camera, UFIR filter, cUFIR filter, UFIR/cUFIR filter and the reference value.

posed UFIR/cUFIR filter fall in-between. The root mean square errors (RMSE) of the heights measured by the camera, UFIR filter, cUFIR filter, UFIR/cUFIR filter are listed in Fig. 7. In this work, we compute the RMSEs by the following equation:

$$\mathbf{Lo}_k^{RMSE} = \frac{1}{k}\sum_{i=1}^{k}\sqrt{\left(z_k - z_k^r\right)^2}, \qquad (14)$$

where the z_k means the measurement of the height and z_k^r means the reference value of the height, which is measured by the ultrasonic sensor. From Fig. 7, we can see easily that the camera's solution accumulates errors. The UFIR and the cUFIR filters have better performance compared with the camera's solution, and the proposed UFIR/cUFIR filter has the smallest error, which shows the best performance. The cumulative distribution function (CDF) of the the heights measured by the camera, UFIR filter, cUFIR filter, UFIR/cUFIR filter are shown in Fig. 8. From the figure, we can see that the hybrid filter gives the smallest RMSE of 0.9. The height RMSEs produced by the UFIR filter, cUFIR filter, UFIR/cUFIR Filter are listed in Tab. 1. From Table 1, we see that the proposed filter gives the error of 0.010 m, which is better that by the UFIR and cUFIR filters on about 28.57% and 16.67%, respectively.

5 Conclusion

In this study, we proposed a new scheme for INS-assisted visual localization of the autonomous landing of UAVs. Based on the data fusion model, the hybrid UFIR/cUFIR filter has been developed.

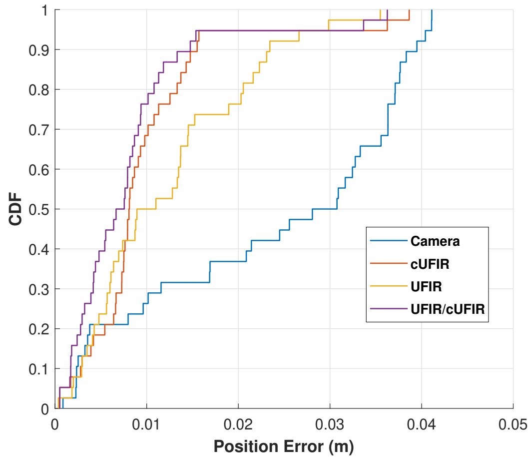

Figure 7: The RMSEs of the heights measured by the camera, UFIR filter, cUFIR filter, UFIR/cUFIR filter.

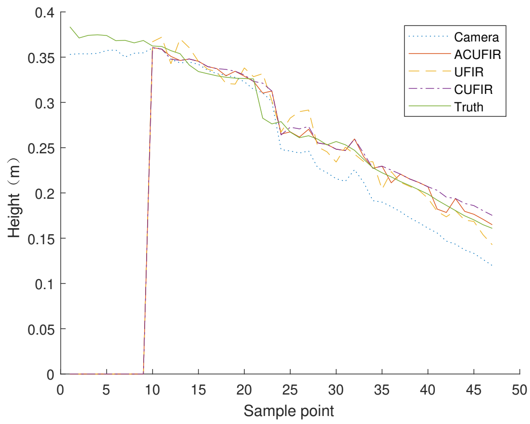

Figure 8: The CDF of the heights measured by the camera, UFIR filter, cUFIR filter, UFIR/cUFIR filter.

Table 1: Height RMSEs Produced by the UFIR filter, cUFIR filter, UFIR/cUFIR Filter.

Filter	RMSE (m)
UFIR	0.014
cUFIR	0.012
UFIR/cUFIR	0.010

In the proposed structure, the conventional UFIR and cUFIR filters are run simultaneously in CMN environment, and the best result of the dynamically selected filter, using the *Mahalanobis* distance, goes to the output. The test results demonstrate that our proposed UFIR/cUFIR filtering algorithm performs better that the UFIR and cUFIR filters, which results in highest positioning accuracy.

References:

[1] A. R. Jha, *Theory, Design, and Applications of Unmanned Aerial Vehicles*. Boca Raton, FL: CRC Press, 2017.

[2] L. Setlak and R. Kowalik, "The dynamics of group flights of an unmanned aerial vehicle," *WSEAS Trans. Appl. Theor. Mech.*, vol. 14, pp. 129–139, 2019.

[3] X. Gao, Z. Chen, and Y. Hu, "Analysis of unmanned aerial vehicle MIMO channel capacity based on aircraft attitude," *WSEAS Trans. Inform. Sci. Appl.*, vol. 10, no. 2, pp. 58–67, 2013.

[4] P. Wilson, *Surviving with Navigation & Signaling*. Broomall, PA: Simon & Schuster, 2015.

[5] R. Perry, *A History of Satellite Reconnaissance*. Chantilly, VA: CSNR, 2015.

[6] B. C. Williams and G. C. Baker, "An electromagnetic induction technique for reconnaissance surveys of soil salinity hazards," *Australian Journal of Soil Research*, vol. 20, no. 2.

[7] X. Dong, Y. Gao, J. Guo, S. Zuo, J. Xiang, D. Li, and Z. Tu, "An integrated UWB-IMU-vision framework for autonomous approaching and landing of UAVs," *Aerospace*, vol. 9, no. 12, pp. 6336–6350, 2022.

[8] Y. Xu, D. Wan, S. Bi, H. Guo, and Y. Zhuang, "A FIR filter assisted with the predictive model and ELM integrated for UWB-based quadrotor aircraft localization," *Satellite Navigation*, vol. 4, p. 2, 2023.

[9] C. Z. L. Huang, J. Song and G. Cai, "Observable modes and absolute navigation capability for landmark-based IMU/vision navigation system of UAV," *Optik*, vol. 202, p. 163725, 2020.

[10] Y. Xu, D. Wan, Y. S. Shmaliy, X. Chen, T. Shen, and S. Bi, "Dual free-size LS-SVM assisted maximum correntropy Kalman filtering for seamless INS-based integrated drone localization," *IEEE Trans. Ind. Electron.*, 2023.

[11] X. Liang, G. Chen, S. Zhao, and Y. Yu, "Moving target tracking method for unmanned aerial vehicle/unmanned ground vehicle heterogeneous system based on AprilTags," *Meas. Control*, vol. 53, no. 3-4, pp. 427–440, 2020.

[12] C. Huang and G. Cai, "Design and performance analysis of landmark-based INS/vision navigation system for UAV," *Optik*, vol. 172, pp. 484–493, 2018.

[13] J.-P. Condomines, *Nonlinear Kalman Filtering for Multi-Sensor Navigation of Unmanned Aerial Vehicles*. London: Elsevier, 2018.

[14] M. H. Sadraey, *Design of Unmanned Aerial Systems*. Hoboken, NJ: Wiley, 2020.

[15] F. L. Lewis, L. Xie, and D. Popa, *Optimal and Robust Estimation*. Boca Raton, FL: CRC Press, 2008.

[16] Y. S. Shmaliy and S. Zhao, *Optimal and Robust State Estimation: Finite Impulse Response (FIR) and Kalman Approaches*. New York: Wiley & Sons, 2022.

[17] Y. Xu, Y. S. Shmaliy, Y. Li, and X. Chen, "UWB-based indoor human localization with time-delayed data using EFIR filtering," *IEEE Access*, vol. 5, pp. 16676–16683, 2017.

[18] Y. Xu, Y. S. Shmaliy, C. K. Ahn, T. Shen, H. Guo, and Y. Zhuang, "Blind robust multi-horizon EFIR filter for tightly integrating INS UWB," *IEEE Sensors J.*, vol. 21, no. 20, pp. 23037–23045, 2021.

[19] Y. S. Shmaliy, S. Zhao, and C. K. Ahn, "Kalman and UFIR state estimation with coloured measurement noise using backward Euler method," *IET Signal Process.*, vol. 14, no. 2, pp. 64–71, 2020.

[20] M.-C. O. S. Popescu, O. V. Olaru, and N. E. Mastorakis, "Processing data for colored noise using a dynamic state estimator," *Int. J. Comp. Commun.*, vol. 2, no. 3, pp. 77–86, 2008.

[21] A. E. Bryson and L. J. Henrikson, "Estimation Using Sampled-Data Containing Sequentially Correlated Noise, Technical Report No. 533," Tech. Rep. NR-372-912, Grant NGR 22-007-068, National Aeronautics and Space Administration, 06 1967.

[22] A. E. Bryson and L. J. Henrikson, "Estimation using sampled data containing sequentially correlated noise," *J. Spacecraft and Rockets*, vol. 5, no. 6, pp. 662–665, 1968.

Contribution of Individual Authors to the Creation of a Scientific Article (Ghostwriting Policy)

The authors equally contributed in the present research, at all stages from the formulation of the problem to the final findings and solution.

Sources of Funding for Research Presented in a Scientific Article or Scientific Article Itself

No funding was received for conducting this study.

Conflict of Interest

The authors have no conflicts of interest to declare that are relevant to the content of this article.